

## DIFFRACTION STUDIES OF RARE EARTH METALS AND SUPERLATTICES

J. BOHR

*Risø National Laboratory, DK-4000 Roskilde, Denmark*

Doon GIBBS and J.D. AXE

*Brookhaven National Laboratory, Upton, NY 11973, USA*

D.E. MONCTON and K.L. D'AMICO

*Exxon Research and Engineering Co., Annandale, NJ 08801, USA*

C.F. MAJKRZAK

*National Institute of Standards and Technology, Gaithersburg, MD 20899, USA*

J. KWO and M. HONG

*AT&T Bell Laboratories, Murray Hill, NJ 07974, USA*

C.L. CHIEN

*Johns Hopkins University, Baltimore, MD 21218, USA*

J. JENSEN

*H.C. Ørsted Institute, Physics Laboratory, DK-2100 Copenhagen Ø. Denmark*

Revised manuscript received 6 February 1989

We review the results of X-ray scattering studies of the rare earth metals and present related new results for superlattices and thin slabs. In rare earth crystals we have observed weak structural modulations which accompany the magnetic ordering. The wave length of this modulation can be derived from a spin-slip model in accordance with symmetry considerations. X-ray scattering of both the charge and magnetization density modulations allow for highly accurate determination of the magnetic wave vector. The physical basis of our discussion is given in the context of lattice modulations. The implications of these results for the understanding of magnetic structure of rare earth superlattices are also discussed in the light of recent neutron diffraction studies of holmium–yttrium superlattices. The effect of the finite size of the magnetic block in a superlattice is considered and it is shown that significantly different behavior than in bulk is expected. In particular it is found that for thin slabs the ferromagnetic phase has the lowest energy.

### 1. Magnetic X-ray scattering

The application of magnetic X-ray scattering techniques as a probe of magnetic structures was pioneered in the successful experiments of De Bergevin and Brunel [1, 2]. Basically electromagnetic waves and hence X-rays will scatter from magnetic structures. For references to detailed calculations of the cross section for magnetic

scattering from solids it should suffice to refer to the more recent work: Platzman and Tozar [3], Blume [4], Moncton et al. [5], Blume and Gibbs [6] and Lovesey [7]. For the practical application of magnetic X-ray scattering techniques the recent discovery of the large enhancement of the cross section found at the absorption edges [8, 9] may be most important having penitential implications for future work in an equally significant

way as the use of circularly polarized beams [10, 11]. In the present context these results are not important and we need only to emphasize that the two linear polarization states mix.

## 2. Holmium

The utilization of magnetic X-ray scattering in the study of the magnetic structures of the rare earth metals was furthered in part by the large localized moment typical of rare earth metals and in part by the high degree of incommensurability between the magnetic structures and the chemical lattice. The magnetic moment in the rare earth metals originates in the unfilled 4f electron shell. A holmium atom has a moment of  $10.3 \mu_B$ . For bulk holmium, which has a hexagonal closed-packed crystal structure, the moments order in an antiferromagnetic spiral made up of ferromagnetically ordered basal planes with moments in successive basal planes rotated relative to each other by the turn-angle of the spiral [12, 13]. This leads to a diffraction pattern with satellites of magnetic origin along the [001] direction above and below the Bragg points of

the crystal lattice. Figure 1 shows a series of X-ray scans of the magnetic satellite above the (004) Bragg points. The peak widths of the satellites are approximately  $0.003 \text{ \AA}^{-1}$ . This demonstrates the high momentum transfer resolution which is available with synchrotron X-ray sources. The count rate was about 40 counts/s [14].

Figure 2 shows the detailed evolution in the magnetic satellite as the temperature is lowered from 25 to 17 K [15]. As the temperature decreases a second, and initially broad, diffraction peak appears on the right side of the magnetic satellite. Because the X-ray magnetic cross section for a magnetic spiral mixes the two polarization states, a polarization sensitive X-ray analyzer can be used to investigate the magnetically scattered intensity in greater detail. For this purpose a graphite crystal was used as a polarization analyzer following a conventional germanium (111) analyzer [5]. By choosing the photon energy, the (006) Bragg reflection in the graphite polarization analyzer could be set at exactly 90 degrees. Then, the polarization analyzer was oriented to pass only photons whose polarization state had been rotated during the

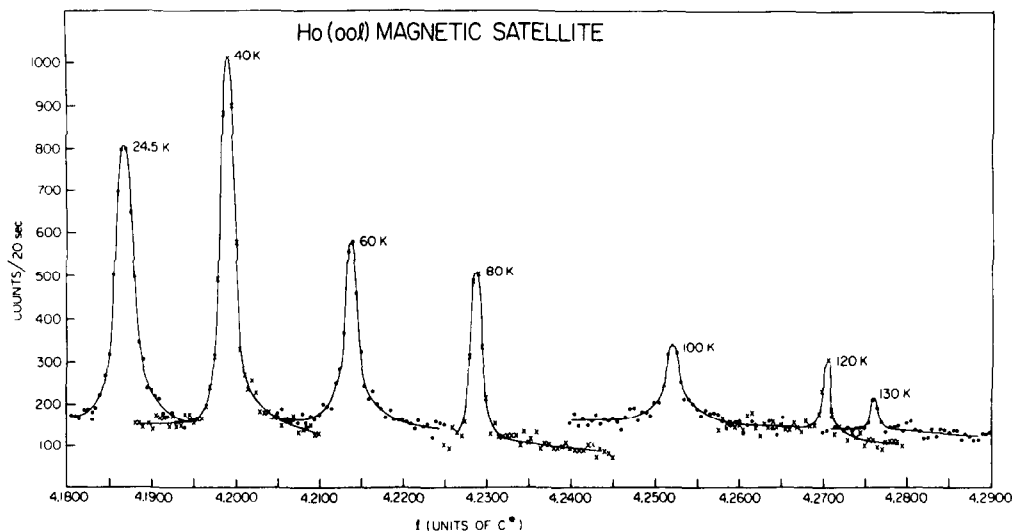


Fig. 1. Magnetic satellites above the (004) Bragg peak at various temperatures as obtained by X-ray diffraction at SSRL using the 54 pole wiggler. The typical peak width is  $0.003 \text{ \AA}^{-1}$  demonstrating the high resolution generally obtained by synchrotron X-ray diffraction.

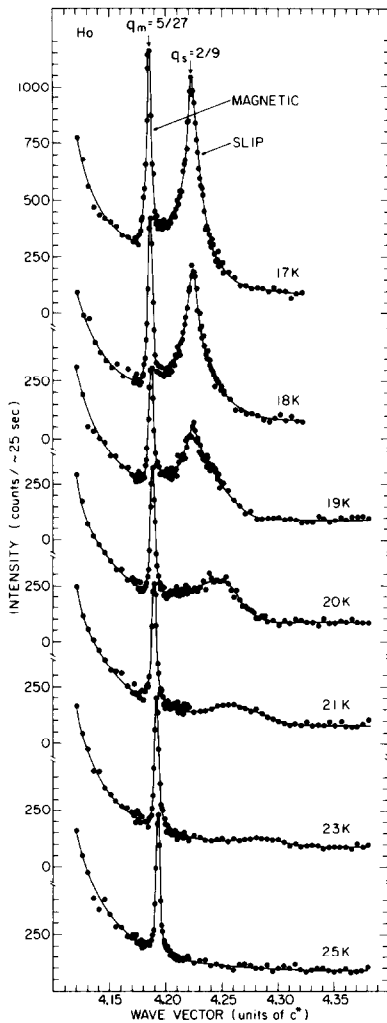


Fig. 2. Detailed temperature development between 25 and 17 K of the magnetic satellite above the (004) Bragg peak. In addition to the sharp magnetic satellite an initially broad second peak appears at a higher wave vector. At lower temperature when the magnetic period approaches 5/27 the additional peak becomes sharper and well defined.

scattering process: i.e., no conventionally Thomson-scattered photons could be detected [14]. Figure 3 shows the diffraction pattern of the satellite at 19 K with and without the polarization analyzer in place. This measurement confirms the magnetic origin of the sharp satellite since some of the scattered photons contributing to this reflection have a rotated polarization state. However, the second and broader diffraction peak is non-magnetic in origin.

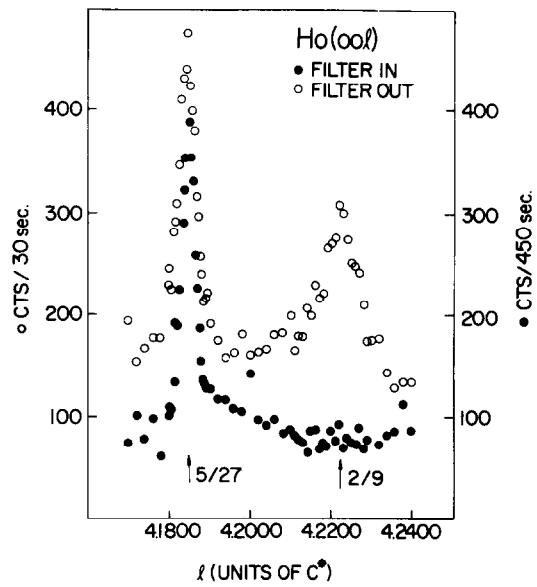


Fig. 3. Diffraction pattern of the magnetic satellite as obtained with and without the polarization analyzer or filter. The open circles are of the scan without the polarization analyzer in place and therefore comprise scattered light with rotated as well as non-rotated polarization. The solid circles are of the scan with the polarization analyzer in place which act as a filter and only passes on to the detector X-rays with a rotated polarization which therefore must have undergone magnetic scattering.

### 3. Spin slips and magnetoelastically induced lattice modulation

The crystal field in the hexagonal basal plane of holmium has six-fold symmetry and, consequently, six easy directions. The crystal field provides a perturbation potential which affects the orientations of the moments within the basal planes. Therefore, the simple antiferromagnetic spiral with the magnetic wave vector  $q_m$  is modulated with the wave vector  $q_s$  [15]:

$$q_s = 12q_m - 2.$$

Briefly, the magnetic moments along the spiral in holmium are bunched or grouped together according to which easy direction the moments are nearest. This leads to spin doublets and occasionally singlets, a doublet being defined

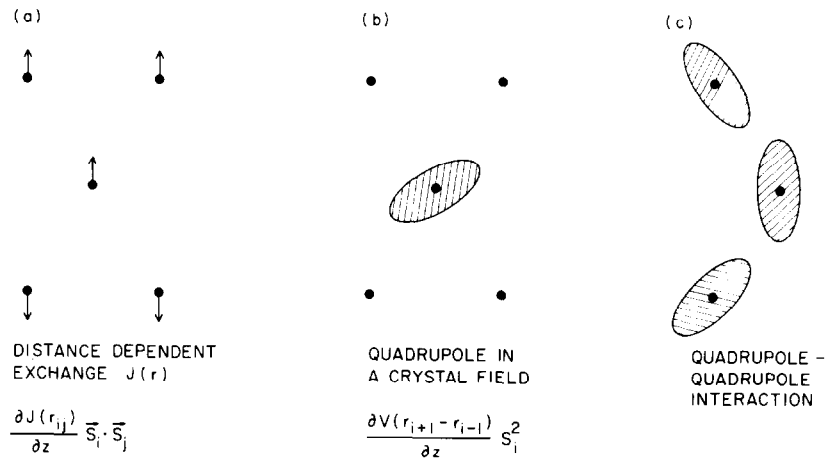


Fig. 4. Schematic of three mechanisms which can lead to lattice modulations: (a) distance dependent exchange, (b) quadrupole in a crystal field, and (c) quadrupole-quadrupole interaction.

when moments in adjacent basal planes are within  $\pm 30$  degrees away from the same easy direction. We have adopted the names *spin-slips* for the singlets and *spin-slip period* for the wave length given by  $q_s$ . As we shall see, for specific temperatures this structural modulation becomes rather sharp and a description in terms of discommensurations becomes appropriate with the singlets being the discommensurations.

The non-magnetic diffraction peak in figs. 2 and 3 occurs at the spin-slip position  $q_s$ . Its relatively large width reveals disorder in the spin-slip distribution of the spiral. When the magnetic period becomes commensurate with the lattice period and there is exactly one spin-slip for every nine atomic layers ( $q_s = \frac{2}{9}$  and  $q_m = \frac{5}{27}$ ), the spin-slip order becomes significantly longer ranged. This is illustrated by the diffraction pattern at 17 K. We interpret the spin-slip diffraction peak as being due to crystal lattice modulations. In view of the large magnetotriction generally found in the rare earth metals we suggest three possible mechanisms shown in fig. 4. The first is a distance-dependent exchange interaction. At spin slip positions the turn angle differs from the turn angles in the rest of the structure. A distance-dependent exchange interaction will therefore lead to lattice modulations which arise from the spin slips. The second mechanism arises directly from the crystal field.

The different orientations of the magnetic moments relative to the crystal field gives rise to local differences in the magnetotriction. The third proposed mechanism is a quadrupole-quadrupole interaction. This mechanism would also give a second harmonic of the magnetic satellite. The modified structure of the magnetic spiral resulting from the crystal field will, in addition to the magnetoelastically induced lattice modulation, give rise to weak magnetic satellites at  $q_m \pm q_s$ . Recently, Cowley and Bates have performed a detailed study of these satellites as well as other harmonics using high resolution neutron diffraction techniques [16].

#### 4. Higher harmonics

The deviation of the magnetic structure from a simple spiral with a constant turn angle leads to the existence of higher harmonics. In the early neutron scattering studies of holmium, Koehler and co-workers [12, 13] observed 5th and 7th harmonics of equal intensity from the low temperature commensurate spiral with a turn angle of 30 degrees. It was shown that this is due to bunching of the moments along the six easy directions. In a later sample, where the low temperature wave vector was close to  $\frac{5}{27}$ , Felcher et al. [17] found that the ratio of intensities of

the 5th to the 7th harmonic was close to 2. Assuming a spin-slip model where the magnetic spiral was considered to consist of doublets and singlets and with the only free parameter being the bunching angle in the doublets, the ratio of the 5th to 7th harmonic has been satisfactorily accounted for [15].

A simple spin-slip model is of course an oversimplification. To obtain a more detailed picture of the spin configuration a molecular or mean field calculation with no adjustable parameters was performed. The molecular field calculation was developed to fit data from a study of spin waves in  $\text{Ho}_{0.9}\text{Tb}_{0.1}$  by Larsen et al. [18]. This molecular field calculation was also applied by Jensen to a study of the spin waves in holmium [19]. We used the parameters found in the study by Larsen et al. with no adjustments, see table I.

Table I

Inter-layer exchange parameters  $J_0$  to  $J_6$  in the molecular field calculations. The crystal-field parameters were  $B_2^0 = 0.024$ ,  $B_4^0 = 0$ ,  $B_6^0 = -0.956 \times 10^{-6}$  and  $B_6^6 = -9.21 \times 10^{-6}$  (x-axis||b-axis, easy), all values given are in meV and the temperature is 4 K.

$J_0$	$J_1$	$J_2$	$J_3$	$J_4$	$J_5$	$J_6$
0.3002	0.0895	0.0065	-0.0121	-0.0055	-0.0010	-0.0030

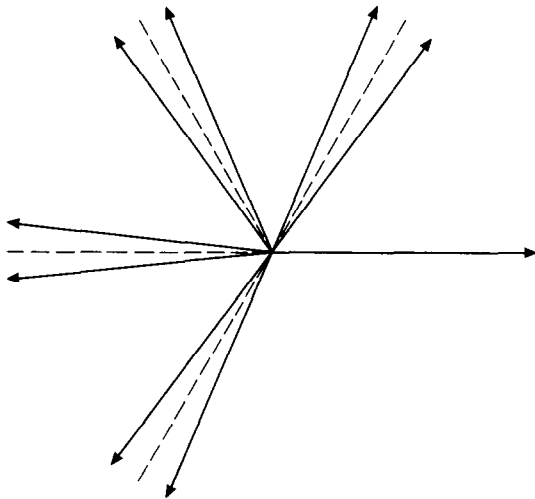


Fig. 5. The spin configuration of the  $q_m = 5/27$  structure as found in the mean field calculation. The first bunching angle is  $13.35^\circ$  while the second is  $12.21^\circ$ . This agrees with the simple spin-slip picture. The dashed lines are the easy directions of the crystal field.

The result for the spin-slip structure which repeats itself for every 9th atomic layer and with  $q_m = \frac{5}{27}$  is given in fig. 5. The 1st bunching angle is  $13.35^\circ$  while the 2nd is  $12.21^\circ$ . The 3rd and 4th bunching angles are, by symmetry equal to the 2nd and 1st, respectively. Thereafter comes a spin-slip followed by a repeat of the 4 doublets. The result of the molecular field calculation is that the bunching angle of the different doublets are very similar, which confirms the simple spin-slip picture with localized discommensurations. The neutron diffraction work by Cowley and Bates [16] with detailed calculations of large number of harmonics comes to a similar result.

## 5. Erbium

Figure 6 shows a summary of the positions of the satellites found in erbium [20]. The situation is considerably more complex for erbium than it is for holmium. There is a large number of harmonics as a result of the frequency mixing between the apparent period of the crystal field and the period of the magnetic structure.

The crystal structure of erbium is also hexagonal closed-packed and the atomic moment is about  $9\mu_B$ . The magnetic ordering on erbium exhibits a variety of phases. Between the Néel temperature of 84 K and 52 K, the magnetic structure is *c*-axis modulated [21–23]. The moments in the basal planes of the hexagonal structure are ordered ferromagnetically in the direction of the *c*-axis with a long wave length modulation along the *c*-axis. The magnetic period is approximately seven atomic planes long. In this temperature interval the only observed X-ray peak along the [001] direction is at  $2q_m$ . The lattice modulation in a *c*-axis-modulated squared-up magnetic structure with fully developed magnetic moments, must be of the kind generated by distance-dependent exchange. However, for sinusoidal magnetic structure all of the three proposed mechanisms; distance dependent exchange, crystal field, and quadrupole-quadrupole interaction, will lead to lattice modulations at  $2q_m$ . In addition, scattering from the

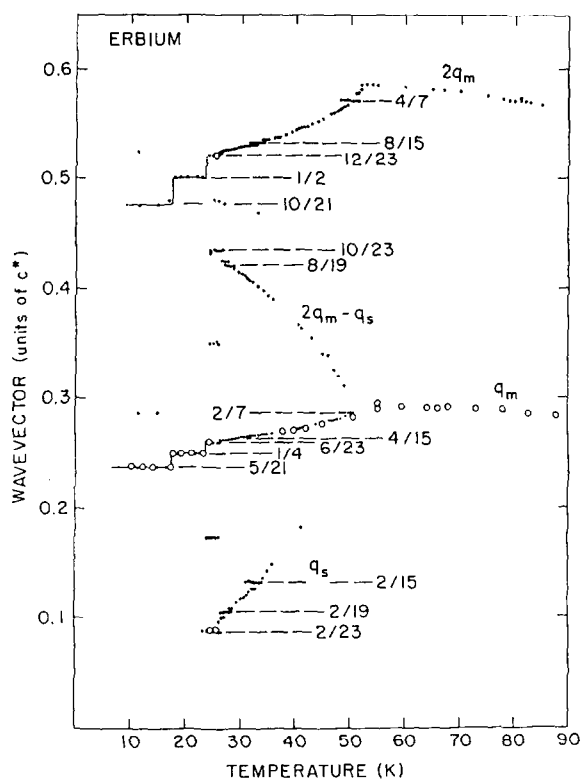


Fig. 6. Positions of the observed diffraction satellites from erbium along the (001) direction. In X-ray scans ( $\cdot$ ) satellites were observed at the magnetic period  $q_m$ , twice the magnetic period  $2q_m$ , the spin-slip period  $q_s$ , its complementary  $2q_m - q_s$  and when the intensity of the spin-slip lattice modulation was significantly pronounced additional harmonics present. The open circles ( $\circ$ ) give the wave vectors observed by neutron diffraction. When  $q_m = 6/23$  the spin-slip modulations were particularly strong and also seen with neutrons.

charge distribution of the quadrupoles will be present at  $2q_m$ .

Between 52 K and 18 K the moments develop an additional basal plane component of identical period to the coexisting  $c$ -axis modulation. The diffraction pattern shows the magnetic period  $q_m$ , twice the magnetic period  $2q_m$ , the spin-slip period  $q_s$  and its complementary period  $2q_m - q_s$ . This is a question of semantics, namely, whether the spin-slips, *blocks of 3 spins*, or *blocks of 4 spins* are to be considered the discommensurations [15]. In erbium blocks of 3 spins and blocks of 4 spins orientated parallel or anti-parallel to the  $z$ -axis, are the fundamental

building blocks, in analogy to the singlets and doublets in holmium. At the lower temperatures, additional harmonics develop, signifying an increased distortion [20]. Below 18 K the magnetic structure becomes a conical spiral. Summarizing, in the entire temperature range the magnetic period exhibits a sequence of first-order transitions to the commensurate wave vectors  $\frac{2}{7}$ ,  $\frac{4}{15}$ ,  $\frac{6}{23}$ ,  $\frac{1}{4}$  and  $\frac{5}{21}$ . This phenomenon is reminiscent of an incomplete devil's staircase [24]. In the low temperature  $\frac{5}{21}$  conical phase of erbium we observe a

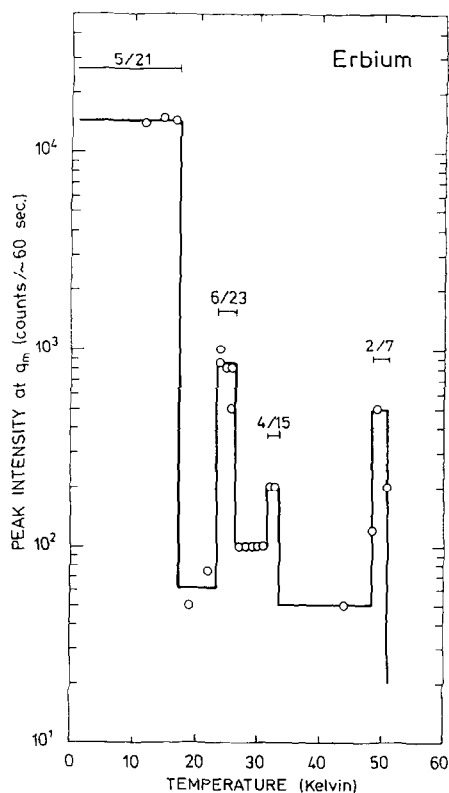


Fig. 7. Peak intensity of the fundamental  $q_m$  as function of temperature. Note the large variations in the intensity over more than 2 orders of magnitude. The intensity is enhanced at temperatures where the magnetic wave vector corresponds to a structure with a ferromagnetic component. For those structures the inversion symmetry of the magnetic structure is broken and consequently charge scattering is allowed at the fundamental  $q_m$ . The  $2/7$  structure has 3 spins up for every 4 spins down. The  $4/15$  structure has 3 spins up followed by 4 spins down, 4 spins up and 4 spins down, this structure then repeats itself. The  $6/23$  structure is the next ferromagnetic structure generated in this way. Finally, the  $5/21$  structure is the conical structure which occurs below the Curie point.

dramatic increase by two orders of magnitude in the peak intensity at  $q_m$ . This signal seems to be too large to result from magnetic scattering alone and suggests the possibility of additional charge scattering appearing at the magnetic wave vector. Figure 7 shows the peak intensity at  $q_m$  as function of temperature on a logarithmic scale. In addition to the large enhancement of the scattering at  $q_m$  in the low temperature conical phase, the weakly ferromagnetic phases  $\frac{2}{7}$ ,  $\frac{4}{15}$  and  $\frac{6}{23}$  also shows enhanced scattering at  $q_m$ . If the magnetic structure has a ferromagnetic component then its inversion symmetry is broken and hence the quadrupole charge distribution will generally give rise to charge scattering at the fundamental  $q_m$ . Furthermore, when the inversion symmetry is broken then the three mechanisms for lattice modulations given in fig. 4 can all give rise to charge scattering at  $q_m$ .

## 6. MBE rare earth super lattice structures

A magnificent recent development in materials science is the advanced level which has been achieved technologically to manufacture new materials not naturally available in nature. The technique of molecular beam epitaxy (MBE) has been used to grow single-crystal rare earth superlattices of high perfection [25]. Magnetic structures consisting of a discrete number of alternating magnetic and nonmagnetic layers such as, for example,  $\text{Ho}_{15}\text{-Y}_{12}$  have been grown. The significant finding that, despite the relatively thick layers of magnetically dead material, the magnetic structure in the superlattice can still exhibit long-range order [26], has given impetus to the study of superlattices of rare earth metals.

## 7. Holmium–Yttrium data

Yttrium, with its lack of 4f electrons, normally does not exhibit magnetism. Therefore, yttrium is often chosen as the component for the magnetically dead layers. Holmium, with its large magnetic moment and its well characterized magnetic spiral, is an ideal element to use for the magnetic

layers. It is unknown how the magnetic interaction propagates through the yttrium layer. This is an important question for the understanding of the magnetic phases in the rare earth superlattices. Several qualified suggestions for the mechanism have been put forward [27]. Is the usual RKKY (Ruderman–Kittel–Kasuya–Yosida) indirect exchange dominant? Is there an itinerant spin density wave in the yttrium layers? For example, alloying yttrium with a few percent dysprosium is enough to magnetize it in a helical way [28, 29]. It seems that this is in general true in the dilute dysprosium limit. Although smaller, the average dysprosium-dysprosium neighbor distance in these alloys is of the same order of magnitude as the thickness of the yttrium layer in the superlattice.

## 8. Finite-sized magnetic structures

Although our knowledge of the magnetic interactions in the superlattice is limited, we can assume that the interaction through the nonmagnetic yttrium layers is much weaker than the interactions in the magnetic holmium layers. Therefore, the magnetic structure in a single block of holmium layers (to a good approximation) may be described as if there were only these internal holmium interactions present. Of course the strain present in the MBE sandwich influences these interactions.

A beginning to an understanding of the magnetic structure of a finite block of atoms can be acquired in the following way. For the infinite spiral structure, the minimum model with enough ingredients to lead to a long period spiral, is one where the exchange interaction  $J_1$  between nearest-neighbor planes is ferromagnetic and the exchange interaction  $J_2$  between next-nearest-neighbor planes is antiferromagnetic. (The indirect exchange found in the rare earth metals is of course of much longer range.) In this simple model we get the well-known result that if  $|J_1/J_2| < 4$ , then the structure is a spiral with a turn angle  $\alpha$  given by  $\cos \alpha = |J_1/4J_2|$ . If on the other hand  $|J_1/J_2| \geq 4$  then the spin organization is ferromagnetic. Turn angle  $\alpha$

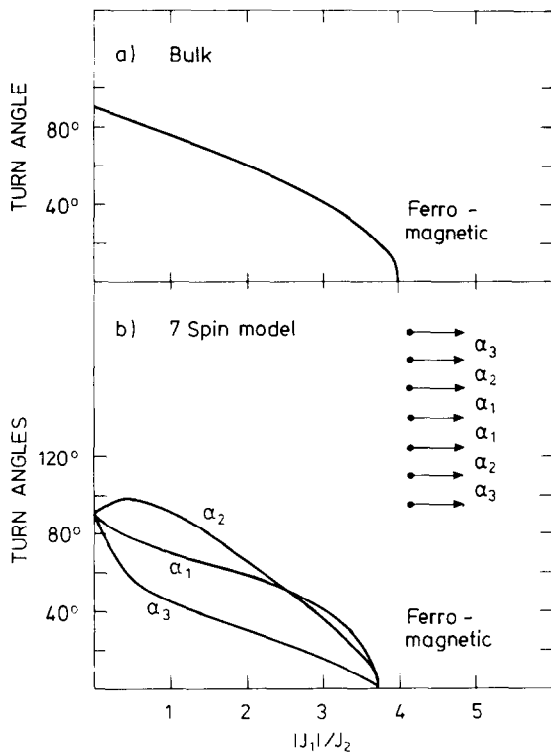


Fig. 8. Turn angles as calculated from a simple model involving ferromagnetic nearest layer interactions and antiferromagnetic next-nearest-layer interactions described by the two exchange constants  $J_1$  and  $J_2$ . (a) The well known result  $\cos \alpha = |J_1/J_2|$  for a model with an infinite number of atomic layers. (b) The three turn angles  $\alpha_1$ ,  $\alpha_2$  and  $\alpha_3$  describing the spin configuration for a model with only 7 atomic layers.  $\alpha_1$  being the inner most turn angle,  $\alpha_2$  the next inner one, and  $\alpha_3$  the outer most turn angle, see inset of model in the figure.

calculated as a function of  $|J_1/J_2|$  is shown in fig. 8a.

Now, consider a finite slab of basal planes instead of an infinite sequence. Then the magnetic structure found by minimization of the simple Hamiltonian will be significantly distorted from the simple spiral. For instance, a block consisting of only 2 basal planes is always ferromagnetic! A detailed calculation of the turn angles in a block of 7 spins is shown in fig. 8b. When  $|J_1/J_2| \geq 3.75$  this structure is ferromagnetic. For a block with 3, 4, 5 or 6 spins the structure is ferromagnetic when  $|J_1/J_2| \geq 2, 3, 3.45$  and  $3.65$ , respectively. Further, there is a general tendency to approach ferromagnetism

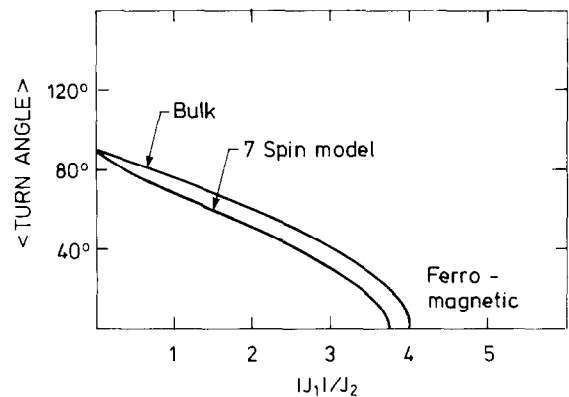


Fig. 9. Average turn angle in the model with 7 spins compared with the turn angle in the infinite model.

for the spins at the edges of a block. Heuristically, this can be understood simply by noting that when  $|J_1/J_2| > 1$  then the nearest neighbor interactions dominates.

The sum of the turn angles over a full block is therefore smaller than the sum over the same number of planes in an infinite structure. Figure 9 demonstrates this in a comparison of the average turn angle in the 7-layer model with the turn angle of the bulk model.

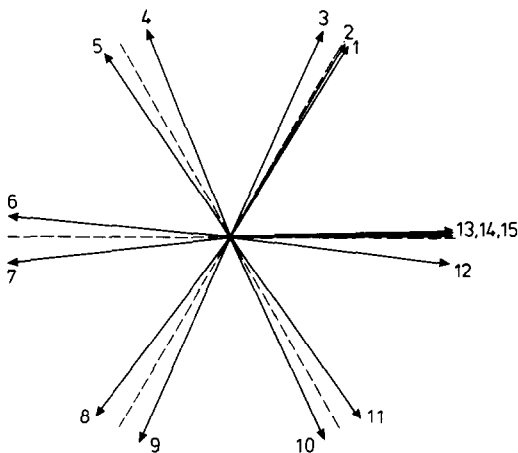
## 9. A realistic mean-field calculation

As was done for the infinite  $q_s = \frac{2}{9}$  spin-slip structure of holmium ( $q_m = \frac{5}{27}$ ), realistic mean field calculations for finite sized holmium blocks can be achieved using the parameters from the work of Larsen et al. [18] (table I). This molecular field Hamiltonian includes interactions up to the 6th nearest neighbor plane. The result for a slab of 15 infinite holmium layers is given in table II and is illustrated in fig. 10. The parameters used are those for the 4 K bulk structure of holmium with a turn angle of 30 degrees. The sum of the 14 turn angles in this calculation is 302 degrees compared with 420 degrees for 15 atomic layers of bulk holmium. From fig. 10 we observe that the tendency to ferromagnetism for the outer most spins is further enhanced by the crystal field. Figure 11 shows a comparison between the calculated energies for the ferromag-

Table II

Mean field calculation of the spins in a slab of 15 layers of holmium atoms using the parameters in table I from ref. [18]. The first column gives the index of the atomic plane. The second and third give the inplane and the z-axis component of the moment, respectively. The fourth column gives the turn angle of the moment. Note that the spin configuration of this holmium slab with an odd number of layers terminates with a triplet and a quartet.

Spin	$S_{  } (\mu_B)$	$S_{\perp} (\mu_B)$	Angle (deg)
1	9.83	1.10	-1
2	9.84	1.32	0
3	9.76	1.85	5
4	9.66	2.27	53
5	9.69	2.16	66
6	9.72	2.02	114
7	9.74	1.92	126
8	9.75	1.90	174
9	9.74	1.94	185
10	9.69	2.14	234
11	9.67	2.21	247
12	9.74	1.90	294
13	9.84	1.33	300
14	9.86	1.11	301
15	9.84	1.01	301



SLAB OF 15 HOLMIUM LAYERS

Fig. 10. The spin configuration with the minimum energy for a slab of 15 atomic layers as found in the mean field calculation. Note the tendency to near ferromagnetism at the outer most atomic layers, i.e. the first 3 layers (1, 2 and 3) and the 4 last layers (12, 13, 14 and 15).

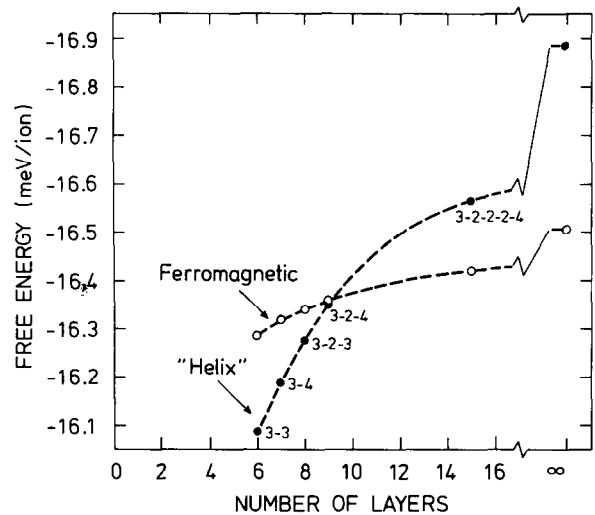


Fig. 11. Free energy per ion for a ferromagnetic and a "helix" structure as calculated in the mean field approximation. For layer thicknesses of less than 9 atoms thick the ferromagnetic configuration is the favored one. The specific configuration of the helix is given by the numbers at the different points of the curve. For example 3-3 means a triplet of spins followed by a triplet.

netic structure and for a spiral structure extending over 2 adjacent easy directions. Interestingly, we observe that for a block of size up to 9 atomic layers thick the favored magnetic configuration is the ferromagnetic state. Experimental observations of turn angles in superlattices different from those in bulk may thus be seen, firstly, as a consequence of the finite size of the magnetic blocks, and, secondly, as a consequence of the perturbation of basic physical parameters such as the strain and interlayer diffusion often present in MBE grown superlattices.

## 10. Experimental structures factors

The experimental structures factors are easily understood. The superlattices can be thought of as a large unit cell in which the magnetic block takes the place of a huge magnetic molecule. The magnetic intensity then occurs at positions determined from the turn angle  $\Delta$  (the phase advance over one large chemical unit cell) as satellites displayed by the corresponding wave

vector  $q_\Delta$  from the reflections corresponding to the large chemical unit cell. When the magnetic order is of long range, the chirality of the magnetic structure is uniquely related to the chirality of the magnetic molecule (single block of magnetic atomic planes). The structure factor is

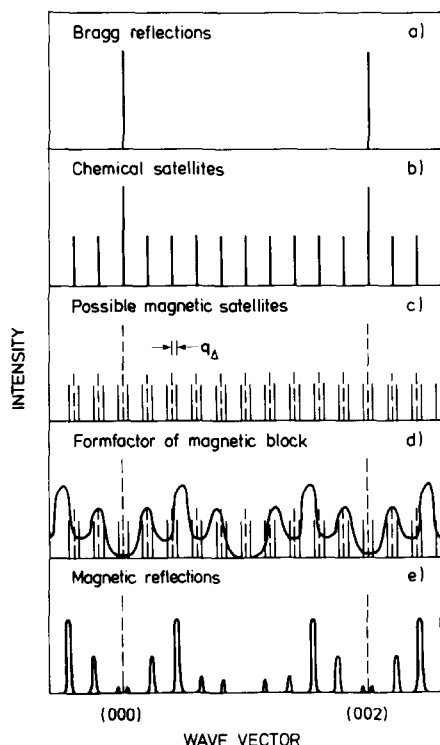


Fig. 12. Schematic explanation of the magnetic reflections from a superlattice with long-range magnetic order. (a) The Bragg reflections from the hexagonal crystal lattice given the inter-layer distance between atomic planes. (b) The chemical satellites representing the length of the large unit cell of the superlattice. (c) The possible positions of the magnetic satellites. It is the first harmonics displaced to both sides of the chemical satellites according to the turn angle  $\Delta$ , where  $\Delta$  is the phase shift of the magnetic structure from one magnetic block to the next. (d) The form factor of one magnetic block. The finite size of a magnetic block gives rise to its oscillator behavior, although the intensity of the side oscillations has been exaggerated in the figure. The true shape of the form factor requires an accurate knowledge of the magnetic structure of the finite block. (e) The magnetic reflections from the superlattice. They arrive from the intersection of the form factor and the magnetic satellites. Note that because the chirality of the magnetic blocks and the chirality of the superlattices are uniquely related only half of the possible magnetic satellites are different from zero.

therefore only non-zero at one of the two possible positions, see fig. 12. As can be seen, the center of mass of the magnetic reflections in fig. 12e) is generally different from the center of the formfactor fig. 12d). This has the consequence that the magnetic turn angles between atomic layers can not be determined solely from peak positions. In contrast the phase advance  $\Delta$  over a magnetic block and an adjacent nonmagnetic block is directly given by the peak positions of the magnetic reflections.

Figure 13 shows the neutron diffraction pattern as obtained from  $\text{Ho}_{27}\text{-Y}_3$  superlattice at 10 K. The features of the pattern are as discussed in fig. 12e. Although not visible on the scale of fig. 13, we have also observed fifth and seventh harmonics of the principle magnetic scattering in these samples. The drawing on the right on fig. 13 shows schematically the magnetic structure of a superlattice, in this case a  $\text{Ho}_{15}\text{-Y}_{12}$ . By analyzing the peak positions in the diffraction pattern,  $\Delta$ , the magnetic phase advance over one large chemical unit cell, can be determined.

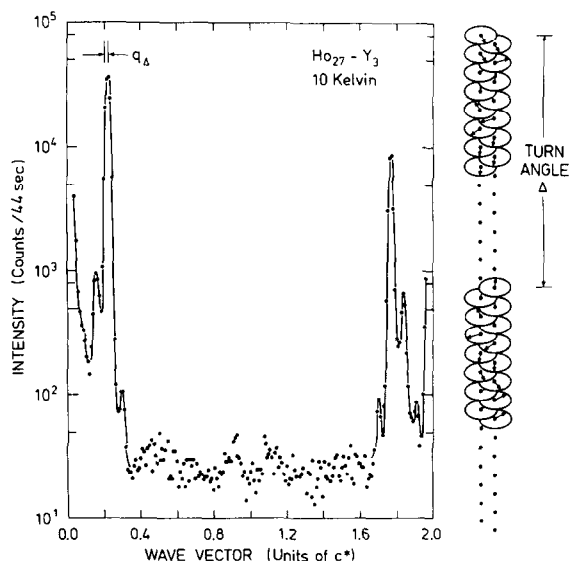


Fig. 13. Neutron diffraction pattern obtained from the  $\text{Ho}_{27}\text{-Y}_3$  superlattice at 10 K. The features of the diffraction pattern are as in figure 12e showing long range magnetic order. On the right side of the figure is shown a schematic drawing of a superlattice explaining the phase advance  $\Delta$ . The data were taken at Brookhaven on the H9 instrument at the cold source at the HFBR.

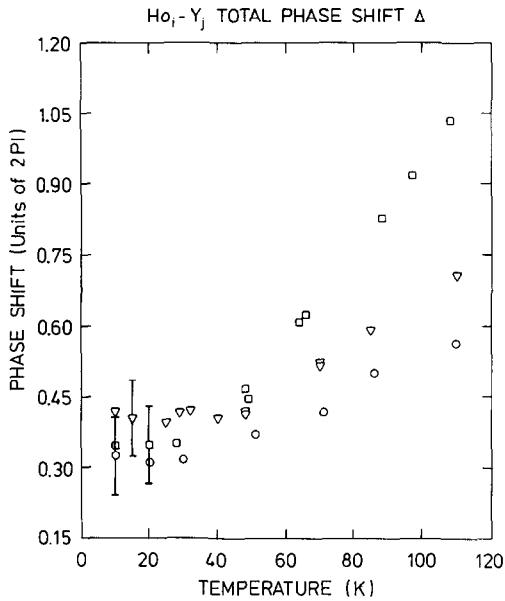


Fig. 14. The phase shift  $\Delta$  from one magnetic block to the next in holmium–yttrium superlattices. The circles ( $\circ$ ) are the data for  $\text{Ho}_{27}\text{-Y}_3$ , the squares ( $\square$ ) for  $\text{Ho}_{15}\text{-Y}_3$  and the triangles ( $\nabla$ ) for  $\text{Ho}_{15}\text{-Y}_{12}$ .

Figure 14 shows the obtained magnetic phase advance  $\Delta$  for the 3 superlattices  $\text{Ho}_{27}\text{-Y}_3$ ,  $\text{Ho}_{15}\text{-Y}_3$  and  $\text{Ho}_{15}\text{-Y}_{12}$ . Because of the relatively large length scale on play in these systems high resolution studies are essential. In fact the resolution of the present study is only barely satisfactory. This manifests itself in the relatively large error bars in fig. 14. Table III gives the phase advance  $\Delta$  as calculated at 10 K assuming triplets or quartlets at the interfaces, doublets in the bulk of the holmium blocks and an anti-

ferromagnetic interaction through the yttrium layers. For the superlattices with thin yttrium blocks this value of  $\Delta$  is in agreement with the experimental value. Thus, it is plausible that the interaction through an  $\text{Y}_3$  block is antiferromagnetic. In gadolinium–yttrium superlattices it has been found that the interaction through the yttrium is always ferromagnetic or antiferromagnetic [30–32]. The result of the molecular field calculation, namely, that the holmium blocks have a tendency to terminate with 3–4 ferromagnetic layers means that possibly the interaction through the yttrium layers is similar to the interaction through yttrium layers in gadolinium–yttrium superlattices, where the gadolinium layers are always ferromagnetic.

## 11. Two types of lack of long-range order

For superlattices with a thicker block of non-magnetic yttrium, for example  $\text{Dy}_{13}\text{-Y}_{42}$ , the magnetic order need not be of very long range [33]. The lack of long-range order in such samples can be due to two distinct types of disorder which we will label type A and B. In type A the disorder is due to the introduction of some randomness in the phase relation between successive magnetic blocks. In type B the disorder appears as a result of some randomness in the type of chirality a magnetic block has. We note that type B disorder leads to a lack of long-range order even if there is a completely deterministic phase relation between neighboring magnetic blocks. It therefore has the attractive physical

Table III

Estimate of the phase advance  $\Delta$  if the interaction through the yttrium layers are assumed to be antiferromagnetic. Column 2 gives the assumed magnetic structure in terms of doublets, triplets and quartets. Column 3 gives the corresponding total turn angle over one holmium block. Column 4 gives the estimated phase advance  $\Delta$  modulus 360 degrees. It should be compared with the  $\Delta$  as extracted from the neutron diffraction data, column 5. All units are in degrees and the data are at 10 K. As can be seen higher resolution data are needed in order to conclude on the nature of the interaction through the yttrium layers.

Superlattices	Ho structure	Turn angle Ho	$\Delta$ (estimated)	$\Delta$ (experimental)
$\text{Ho}_{27}\text{-Y}_3$	322222222224	660	120	116
$\text{Ho}_{15}\text{-Y}_3$	322224	300	120	120
$\text{Ho}_{15}\text{-Y}_{12}$	322224	300	120	150

property that the resulting magnetic order is a genuinely intrinsic metastable configuration. In contrast, for type A disorder the lack of long-range order is most likely extrinsic, due to impurities, lattice imperfections, etc. Metastable locking in the crystal field can also be the cause of type A disorder, but if so type B disorder is most certain to be present, in addition. Moreover, one may argue that tendency to ferromagnetism at the termination of the magnetic blocks provide some extent of screening of the chirality–chirality interaction, lowering the effective chirality–chirality exchange.

## 12. Conclusion

This paper reviews a rather broad spectrum of magnetic structures of bulk rare earth and rare earth superlattices. The emphasis has been to touch on some rather simple and interesting phenomena. We have learned that the lock-in transitions of the magnetic wave vector can be explained as being due to intrinsic structural properties of the magnetism of the rare earth metals involving discommensurations. Therefore, these lock-in transitions shall not be considered to arise from metastable configurations stabilized by impurities and lattice imperfections. In contrast, the effect of impurities and lattice imperfections has no greater effect than to modify the basic physical properties in a mean field manner. Thus the low temperature value of the wave vector may change with the concentration of impurities, but the physics leading to its value is genuine.

For superlattices we can ask a similar question: what is the influence of imperfect growth, interlayer diffusion and lattice strain? The fact that only a finite number of magnetic layers is involved leads to large deviations from bulk behavior. This phenomenon has to be considered prior to the possible effects of the imperfectness of the lattice. Likewise, the finite size of the yttrium slab is important to consider when the interaction through the yttrium is to be understood. Although it has been found that dilute dysprosium–yttrium bulk alloys have helical

order with a turn angle of approximately fifty degrees [28, 29] the helical order need not be the favored state for a thin slab.

We also point out the fact that the lack of long-range order in superlattices with very thick intervening layers of yttrium may be due to near frustration in chirality–chirality correlations. This leads to a diffraction peak whose width is distinctively different from the width corresponding to complete randomness. Work on these and other subjects touched in this paper is in progress.

## Acknowledgements

We wish to thank K.N. Clausen for his careful reading of this manuscript. This work was supported in part by the Danish Natural Science Council. Work performed at Brookhaven is supported by the DOE under contract No. DE-AC02-76CH00016. One of us (JB) also wish to thank the Thomas B. Thrige Foundation.

## References

- [1] F. de Bergevin and M. Brunel, *Phys. Lett A* 39 (1972) 141.
- [2] F. de Bergevin and M. Brunel, *Acta Crystallogr. A* 37 (1981) 324.
- [3] P.M. Platzman and N. Tzaor, *Phys. Rev. B* 2 (1970) 3556.
- [4] M. Blume, *J. Appl. Phys.* 57 (1985) 3615.
- [5] D.E. Moncton, D. Gibbs and J. Bohr, *Nucl. Inst. and Meth. A* 246 (1986) 839.
- [6] M. Blume and D. Gibbs, *Phys. Rev. B* 37 (1988) 1779.
- [7] S.W. Lovesey, *J. Phys. C* 20 (1987) 5625.
- [8] D. Gibbs, D.R. Harshman, E.D. Isaacs, D.B. McWhan, D. Mills and C. Vettier, *Phys. Rev. Lett.* 61 (1988) 1241.
- [9] J.P. Hannon, G.T. Trammell, M. Blume and D. Gibbs, *Phys. Rev. Lett.* 61 (1988) 1245.
- [10] P.M. Brunel, G. Patrat, F. de Bergevin, F. Rousseau and M. Lemmonnier, *Acta Crystallogr. Sect. A* 39 (1983) 84.
- [11] M.J. Copper, D. Laundy, D.A. Cardwell, D.N. Timms, R.S. Holt and G. Clark, *Phys. Rev. B* 34 (1986) 5984.
- [12] W.C. Koehler, J.W. Cable, M.K. Wilkinson and E.O. Wollan, *Phys. Rev.* 151 (1966) 414.
- [13] W.C. Koehler, J.W. Cable, H.R. Child, M.K. Wilkinson and E.O. Wollan, *Phys. Rev.* 158 (1967) 450.

- [14] D. Gibbs, D.E. Moncton, K.L. D'Amico, J. Bohr and B.H. Grier, *Phys. Rev. Lett.* 55 (1985) 234.
- [15] J. Bohr, D. Gibbs, D.E. Moncton and K.L. D'Amico, *Physica A* 140 (1986) 349.
- [16] R.A. Cowley and S. Bates, *J. Phys. C* 21 (1988) 4113.
- [17] G.P. Felcher, G.H. Lander, T. Arai, S.K. Sinha and F.H. Spedding, *Phys. Rev. B* 13 (1976) 3034.
- [18] C.C. Larsen, J. Jensen and A.R. Mackintosh, *Phys. Rev. Lett.* 59 (1987) 712.
- [19] J. Jensen, *J. de Phys.* (to be published).
- [20] D. Gibbs, J. Bohr, J.D. Axe, D.E. Moncton and K.L. D'Amico, *Phys. Rev. B* 34 (1986) 8182.
- [21] J.W. Cable, E.O. Wollan, W.C. Koehler and M.K. Wilkinson, *Phys. Rev.* 140 (1965) A1896.
- [22] M. Habenschuss, C. Stassis, S.K. Sinha, H.W. Deckman and F.H. Spedding, *Phys. Rev. B* 10 (1974) 1020.
- [23] M. Atoji, *Solid State Commun.* 14 (1974) 1047.
- [24] P. Bak, *Rep. Prog. Phys.* 45 (1982) 587.
- [25] J. Kwo, D.B. McWhan, M. Hong, E.M. Gyroy, L.C. Feldman and J.E. Cunningham, in: *Layered Structures, Epitaxy and Interfaces*, eds. J.H. Gibson and L.R. Davidson, *Materials Research Society Symposia Proceedings* 37 (1985) 509.
- [26] M.B. Salamon, S. Shina, J.J. Rhyne, J.E. Cunningham, R.W. Erwin, J. Borchers and C.P. Flynn, *Phys. Rev. Lett.* 56 (1986) 259.
- [27] Y. Yafet, *J. Appl. Phys.* 61 (1987) 4058.
- [28] H.R. Child, W.C. Koehler, E.O. Wollan and J.W. Cable, *Phys. Rev. A* 138 (1965) 1655.
- [29] J.A. Gotaas, J.J. Rhyne, L.E. Wenger and J.A. Mydosh, *J. Appl. Phys.* 63 (1988) 3577.
- [30] C.F. Majkrzak, J.W. Cable, J. Kwo, M. Hong, D.B. McWhan, Y. Yafet, J.V. Waszczak and C. Vettier, *Phys. Rev. Lett.* 56 (1986) 2700.
- [31] J. Kwo, M. Hong, F.J. DiSalvo, J.V. Waszczak and C.F. Majkrzak, *Phys. Rev. B* 35 (1987) 7295.
- [32] C.F. Majkrzak, D. Gibbs, P. Boni, A.I. Goldman, J. Kwo, M. Hong, T.C. Hsieh, R.M. Fleming, D.B. McWhan, Y. Yafet, J.C. Cable, J. Bohr, H. Grimm and C.L. Chien, *J. Appl. Phys.* 63 (1988) 3447.
- [33] M. Hong, R.M. Fleming, J. Kwo, L.F. Schneemyer, J.V. Waszczak, J.P. Mannaerts, C.F. Majkrzak, D. Gibbs and J. Bohr, *J. Appl. Phys.* 61 (1987) 4052.